Inorg. Chem. **2004**, *43*, 8479–8489

Is the Enthalpy of Fusion of Tris(acetylacetonato)metal(III) Complexes Affected by Their Potential Energy in the Crystal State?

Jasmina Sabolović,*,† Željko Mrak,‡ Sanja Koštrun,§ and August Janeković‡

Department of Chemistry, Faculty of Pharmacy and Biochemistry, University of Zagreb, Ante Kovačića 1, HR-10000 Zagreb, Laboratory of Molecular Modeling Chemistry, PLIVA—Research Institute Ltd., Baruna Filipovića 29, HR-10000 Zagreb, and Institute for Medical Research and Occupational Health, Ksaverska cesta 2, P.O. Box 291, HR-10001 Zagreb, Croatia

Received August 10, 2004

In this Article we present enthalpies of fusion and melting points obtained from new thermochemical measurements of tris(acetylacetonato)metal(III), $M(acac)_3$, complexes (M = Fe, Al, Cr, Mn, Co) using differential scanning calorimetry (DSC) and evaluate them in relation to their different values found in the literature. An enthalpy of fusion of 27.67 kJ mol^{-1} was derived for $Mn(acac)_3$ from a symmetrical DSC thermogram captured for the first time. The enthalpy value was indirectly confirmed with the solubility measurements of $Mn(acac)_3$ in acetylacetone. A hypothesis has been stated that the enthalpy of fusion and the potential energy of $M(acac)_3$ in the crystal state may be related. To calculate molecular in-crystal potential energy, in this Article we proposed a molecular mechanics model for the $M(acac)_3$ class of compounds. Nine X-ray crystal structures of $M(acac)_3$ complexes (M = Fe, Al, V, Mn, Co, Cr, Sc) were included in the modeling. The conformational potential energy was minimized for a molecule surrounded by other molecules in the crystal lattice. The partial charges from two schemes, the electrostatic potential (ESP) fit and the natural population analysis (NPA), were used to construct two types of force fields to examine which force field type would yield a better fit with the experimental thermal properties. The final force fields were named FF-ESP and FF-NPA. Both force field sets reproduced well the experimental crystal data of nine $M(acac)_3$ complexes as well as of tris(3-methyl-2,4-pentanedionato-*O*,*O*′)cobalt(III). Only in-crystal potential energies derived by FF-NPA yielded a significant correlation (correlation coefficient $R = -0.71$) with the measured enthalpies of fusion. The enthalpy of fusion for $Co(acac)_3$ could not be determined experimentally because of simultaneous decomposition and fusion, and it is predicted to be 33.2 kJ mol^{-1} from the correlation regression line.

Introduction

Metal complexes with 2,4-pentanedionato (acetylacetonato, acac) are used as part of a catalyst system for various purposes: for polymerization of propylene and ethylene[1,2] as well as of lactide,[3] for the oxidation of alcohols to aldehydes and ketones,[4] for the autoxidation of ethyl linoleate,[5] for preparation of the sulfoxides of penicillin derivatives,[6] for the syntheses of carbon nanotubes and onion particles,[7] for curing epoxy resins,[8] and for purification of metals by zone melting.[9] The effect of tris(acac) complexes with Al(III), Cr(III), Fe(III), and Co(III) on artificial provocation of rain was studied.[10] Metal acetylacetonates are also used as precursors in the preparation of metal oxide

* Author to whom correspondence should be addressed. E-mail: jasmina.sabolovic@imi.hr. Phone: + 385 1 4673 188. Fax: + 385 1 4673 303.
† Institute for Medical Research and Occupational Health.
‡ University of Zagreb.
§ PLIVA—Research Institute Ltd.

(1) Shin, Y. W.; Nakatani, H.; Uozumi, T.; Liu, B. P.; Sano, T. Nitta, K.; Terano, M. *Polym. Int.* **2003**, *52*, 29−34.
(2) Ban, H. T.; Kase, T.; Murata, M. *J. Polym. Sci., Part A: Polym. Chem.* **2001**, *39*, 3733−3738.
(3) Dobrzynski, P. *J. Polym. Sci., Part A: Polym. Chem.* **2004**, *42*, 1886−1900.
(4) Xu, L.; Trudell, M. L. *Tetrahedron Lett.* **2003**, *44*, 2553−2555.
(5) van Gorkum, R.; Bouwman, E.; Reedijk, J. *Inorg. Chem.* **2004**, *43*, 2456−2458.
(6) Hu, Q. Y.; Zhao, J. Q.; Wang, Y. J.; Zhu, L. D.; Li, M. Q.; Li, G. H.; Wang, Y.; Ge, F. Y. *J. Mol. Catal. A: Chem.* **2003**, *200*, 271−277.
(7) Nasibulin, A. G.; Moisala, A.; Brown, D. P.; Kauppinen, E. I. *Carbon* **2003**, *41*, 2711−2724.
(8) Hamerton, I.; Howlin, B. J.; Jepson, P. *Coord. Chem. Rev.* **2002**, *224*, 67−85.
(9) Varlamova, L. M.; Tananaeva, O. I.; Martynenko, L. I. *Probl. Khim. Primen. β [Beta]-Diketonatov Met., [Mater. Vses. Semin.], 4th, 1978 (1982)* **1982**, 184−199.
(10) Huang, T.; Zhang, Z.; Zou, J. *Kexue Tongbao* **1983**, *28*, 318−319.

10.1021/ic048900u CCC: $27.50
Published on Web 12/03/2004

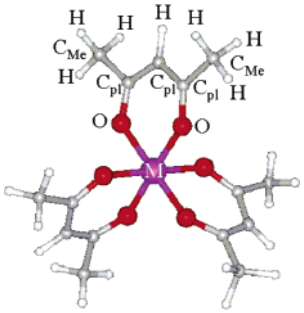

Figure 1. General drawing and atom labeling of the tris(acetylacetonato)-metal(III) complex, M(acac)$_3$, used throughout this Article.

thin films,[11−14] nanoparticles,[15] and nanowires,[16] as well as high-temperature superconducting materials[17] by different metal organic chemical reaction methods.

The X-ray determination and refinement of a number of crystal structures of M^{III}(acac)$_3$ complexes (Figure 1) have made this class of compounds suitable and interesting to gain experimental information on the effects of changing the metal ion and possibly the effect of changing the crystal class, and thus the molecular packing, on the molecular structure.[18−26]

Besides, a number of thermodynamic properties of metal-(III) complexes with acetylacetonates, such as the enthalpy of fusion,[27−31] the melting point,[27,28,30−32] the enthalpies of sublimation,[27,29−31] vaporization,[28,31,33] combustion,[34,35] and formation,[36,37] the heat capacity,[27] and the metal−oxygen thermochemical bond energies,[34,36,37] have been measured to contribute to the knowledge of the physicochemical properties of this class of compounds. However, the reported properties differ in value and measuring procedure.

Significant correlations among boiling point, enthalpy of vaporization, enthalpy of sublimation, and melting point have been established for a wide range of organic and inorganic materials.[38] This result was interpreted so as these four thermodynamic properties provided a measure of the strength of the intermolecular forces. It was also shown that the number and type of intermolecular interactions were likely to be a predominant factor in the volatility of metal complexes with β-diketonates.[39] Volatile trends were established for a series of M(β-diketonato)$_n$ complexes, where M stands for Cu ($n = 2$), Al, Sc, Cr, Fe, Co, and Ga ($n = 3$), and Zr ($n = 4$) and β-diketonato denotes acac, trifluoroacetylacetonato (tfac), hexafluoroacetylacetonato (hfac), and 2,2,6,6-tetramethyl-3,5-heptanedionato (tmhd). Fluorinated complexes are more volatile than nonfluorinated derivates and have lower melting points.[39] For example, the melting points of Sc(acac)$_3$, Sc(tfac)$_3$, and Sc(hfac)$_3$ are 205, 182, and 90 °C, respectively.

The solubility measurements of tris(acac) complexes of Cr(III), Mn(III), Fe(III), and Co(III) in acetylacetone at 20 °C revealed a connection between the solubility and the electronic structure of the central ion.[32] Namely, the maximum solubility was obtained for Mn(acac)$_3$ (high-spin $3d^4$ electronic configuration), and the minimum solubilities were obtained for Cr(acac)$_3$ and Co(acac)$_3$ ($3d^3$ and $3d^6$ electronic configurations, respectively). The result suggested that a relationship among the electronic configuration of the central metal ion, the strength of the metal−oxygen bond, and the solubility of M(acac)$_3$ in acetylacetone might be supposed. As the solubility may also be dependent on the enthalpy of fusion and the melting point,[40] these connections led us to a hypothesis that a correlation between these thermodynamic properties and the energy of M(acac)$_3$ in the solid state may exist.

To obtain the energy of an M(acac)$_3$ complex in the crystal state, we have chosen the molecular mechanics (MM) method. MM force fields (FFs) for modeling metal complexes in the simulated crystalline surroundings are rare[41−47]

(11) Sun, J. B.; Xiong, R.; Wang, S. M.; Tang, W. F.; Tong, H.; Shi, J. *J. Sol-Gel Sci. Technol*. **2003**, *27*, 315−319.
(12) Skordas, S.; Papadatos, F.; Nuesca, G.; Sullivan, J. J.; Eisenbraun, E. T.; Kaloyeros, A. E. *J. Mater. Res.* **2003**, *18*, 1868−1876.
(13) Yasuda, T.; Segawa, Y. *Phys. Status Solidi B* **2004**, *241*, 676−679.
(14) Segura, Y.; Cool, P.; Van der Voort, P.; Mees, F.; Meynen, V.; Vansant, E. F. *J. Phys. Chem. B* **2004**, *108*, 3794−3800.
(15) Sun, S. H.; Zeng, H.; Robinson, D. B.; Raoux, S.; Rice, P. M.; Wang, S. X.; Li, G. X. *J. Am. Chem. Soc.* **2004**, *126*, 273−279.
(16) Chang, K.-W.; Wu, J.-J. *Adv. Mater*. **2004**, *16*, 545−549.
(17) Grigoryan, S.; Manukyan, A.; Hayrapetyan, A.; Arzumanyan, A.; Kuzanyan, A.; Kafadaryan, Y.; Vardanyan, E. *Supercond. Sci. Technol.* **2003**, *16*, 1202−1206.
(18) Hon, P. K.; Pfluger, C. E. *J. Coord. Chem.* **1973**, *3*, 67−76.
(19) Anderson, T. J.; Neuman, M. A.; Melson, G. A. *Inorg. Chem*. **1973**, *12*, 927−930.
(20) Iball, J.; Morgan, C. H. *Acta Crystallogr*. **1967**, *23*, 239−244.
(21) Morosin B. *Acta Crystallogr*. **1965**, *19*, 131−137.
(22) Filgueiras C. A. L.; Horn, A.; Howie, R. A.; Skakle, J. M. S.; Wardell, J. L. *Acta Crystallogr., Sect. E* **2001**, *57*, m157−m158.
(23) Morosin, B.; Montgomery, H. *Acta Crystallogr., Sect. B* **1969**, *25*, 1354−1359.
(24) Fackler, J. P., Jr.; Avdeef, A. *Inorg. Chem*. **1974**, *13*, 1864−1875.
(25) Stults, B. R.; Marianelli, R. S.; Day, V. W. *Inorg. Chem*. **1979**, *18*, 1853−1858.
(26) Abrahams, B. F.; Hoskins, B. F.; McFadyen, D. W.; Perrin, L. C. *Acta Crystallogr., Sect. C* **1998**, *54*, 1807−1809.
(27) Melia, T. P.; Merrifield, R. *J. Inorg. Nucl. Chem*. **1970**, *32*, 2573−2579.
(28) Beech, G.; Lintonbon, R. M. *Thermochim. Acta* **1971**, *3*, 97−105.
(29) Murray, J. P.; Hill, J. O. *Thermochim. Acta* **1983**, *63*, 211−218.
(30) Murray, J. P.; Hill, J. O. *Thermochim. Acta* **1984**, *72*, 341−347.
(31) Lazarev, V. B.; Greenberg, J. H.; Ozerova, Z. P.; Sharpataya, G. A. *J. Therm. Anal*. **1987 (**Publ. **1988)** *33*, 797−799.
(32) Komarov, V. A.; Matveeva, N. I. *Khim. Khim. Tekhnol*. **1974**, *17*, 798−801.
(33) Igumenov, I. K.; Chumachenko, Yu. V.; Zemskov, S. V. *Koord. Khim*. **1979**, *5*, 34−38.
(34) Farran, D. T.; Jones, M. M. *J. Phys. Chem*. **1964**, *68*, 1717−1721.
(35) Cavell, K. J.; Pilcher, G. *J. Chem. Soc., Faraday Trans.* **1977**, *73*, 1590−1594.
(36) Kawasaki, Y.; Tanaka, T.; Okawara, R. *Technol. Rep. Osaka Univ*. **1963**, *13*, 537−562.
(37) Hill, J. O.; Irving, R. J. *J. Chem. Soc. A* **1968**, 1052−1054.
(38) Westwell, M. S.; Searle, M. S. Wales, D. J.; Williams, D. H. *J. Am. Chem. Soc*. **1995**, *117*, 5013−5015.
(39) Fahlman, B. D.; Barron, A. R. *Adv. Mater. Opt. Electron*. **2000**, *10*, 223−232.
(40) Wark, K. Jr.; Richards, D. E. *Thermodynamics*, 6th ed.; WBC/McGraw-Hill: Boston, 1999.
(41) Norrby, P.-O.; Brandt, P. *Coord. Chem. Rev*. **2001**, *212* (1), 79−109.
(42) Sabolović, J.; Tautermann, C. S.; Loerting, T.; Liedl, K. R. *Inorg. Chem*. **2003**, *42*, 2268−2279.
(43) Kaitner, B.; Paulić, N.; Pavlović, G.; Sabolović, J. *Polyhedron* **1999**, *18*, 2301−2311.
(44) Sabolović, J.; Liedl, K. R. *Inorg. Chem.* **1999**, *38*, 2764−2774.
(45) Sabolović, J.; Rasmussen, Kj. *Inorg. Chem.* **1995**, *34*, 1221−1232.
(46) Breu, J.; Domel, H.; Norrby, P.-O. *Eur. J. Inorg. Chem*. **2000**, *11*, 2409−2419.
(47) Mellot-Draznieks, C.; Girard, S.; Ferey, G.; Schon, J. C.; Cancarevic, Z.; Jansen, M. *Chem.—Eur. J.* **2002**, *8*, 4103−4113.

and none of them have been applied to $M^{III}(acac)_3$ complexes so far. Generally, to our best knowledge, only a few MM studies of metal complexes containing acac ligands have been reported; that is, the force field parameters for β-diketonates coordinated to Ti(IV) and Co(III) were developed on the basis of published structural data and the X-ray structures of *cis*-$[Co(acac)_2(NH_3)_2]I\cdot H_2O$ and $[Co(acac)_2$(ethane-1,2-diamine)$]ClO_4$,[48] and the interconversion mechanisms between an idealized square pyramid and two trigonal bipyramids of a five-coordinate $[Ni(acac)_2(py)]$ complex were investigated by combining MM and density functional theory (DFT) approaches.[49] On the other hand, the $M(acac)_3$ compounds have been studied quantum chemically;[50,51] Diaz-Acosta et al. calculated the geometries and IR spectra of trivalent scandium, iron, chromium, and aluminum,[50] as well as titanium, vanadium, manganese, and cobalt[51] tris(acetylacetonate)s using the hybrid density functional method B3LYP[52−55] and compared the derived results with experimental data.

In this Article we present the results of new thermochemical measurements for $M(acac)_3$ complexes (M = Fe(III), Al(III), Cr(III), Mn(III), Co(III)) using differential scanning calorimetry (DSC) and evaluate them in relation to their different values found in the literature.[27−32] An MM model is proposed for this class of compounds. Geometry optimizations were performed in simulated crystalline surroundings. Novel MM force fields were parametrized and examined on available experimental X-ray crystal data. The study is aimed at examining whether a connection between the enthalpy of fusion and the potential energy of the $M(acac)_3$ complexes in the crystal state may be established.

Experimental Section

Materials. $Fe(acac)_3$, $Al(acac)_3$, $Cr(acac)_3$, $Co(acac)_3$, $Mn(acac)_3$, and acetylacetone were purchased from Merck (zur Synthese). The complexes were purified by crystallization in freshly distilled acetylacetone for thermal measurements. In, Sn, Bi, Cd, and Ag_2SO_4 were used as standards to form the thermometric correction curve. They were purchased from NIST (99.9995%).

Thermochemical Measurements. A Perkin-Elmer differential scanning calorimeter (DSC-1B) and TA Instruments DSC 2910 module were used for thermal investigations of metal acetylacetonates in a nitrogen atmosphere in the temperature range from 25 to 300 °C. Since acetylacetonates are volatile and some of them decompose at relatively low temperature or undergo other transformations, high-pressure steel pans in the DSC-1B calorimeter were used throughout for measurements to avoid the influence of sublimation or decomposition. As such high-pressure pans cannot be put into the sample holders of DSC-1B, gold-plated adapters were made for these pans. The following standards were used for the thermometric calibration of the instruments, i.e., to form the thermometric correction curve: In, Sn, Bi, Cd, and Ag_2SO_4. The melting points were corrected by the correction curve. DCS measurements were taken under the following conditions: scanning rate 4 K min^{-1}, sensitivity range 4 mcal s^{-1}, chart speed 20 mm min^{-1}. Indium was used as a calibrant for determination of the enthalpy of fusion, $\Delta_{fus}H$.

Solubility Measurements. An apparatus for the determination of the solubility of pure solid substances in liquid solvents was constructed, and the procedure for setting up complete equilibrium between the solid substance and its solution has been developed.[56] It is intended for work in the temperature range of −30 to +300 °C at atmospheric pressure with optional use of an inert gas.

Theoretical Methods. 1. Quantum Chemical Calculations. The calculations were carried out using the Jaguar suite of programes.[57] The hybrid density functional B3LYP[52−55] was combined with Los Alamos effective core potentials[58] for metal atoms and the 6-31+G* basis set[59−65] for other atoms (LACVP*+ basis set). An unrestricted wave function was used for the open-shell systems. The single-point energy calculations were performed starting from experimental crystal atomic coordinates. Atomic charge distributions were calculated using the electrostatic potential (ESP) fit[66−68] and the natural population analysis (NPA)[69] schemes as implemented in the NBO 5.0 program[70] within the Jaguar suite of programs.

2. MM Model and Calculations. The conformational (strain) potential energy of a molecule was calculated from the following basic formula:

$$V_{total} = \sum_{bonds} D_e(e^{-2\alpha(b-b_0)} - 2e^{-\alpha(b-b_0)}) + \frac{1}{2}\sum_{\substack{valence\\angles}} k_\theta(\theta-\theta_0)^2 + \frac{1}{2}\sum_{\substack{torsion\\angles}} V_\varphi(1 \pm \cos n\varphi) + \frac{1}{2}\sum_{\substack{oop\\torsions}} k_\chi\chi^2 + \sum_{i<j}(A_iA_jr_{ij}^{-12} - B_iB_jr_{ij}^{-6}) + \sum_{l<m} q_lq_mr_{lm}^{-1}$$

Here b, θ, φ, χ, and r are bond lengths, valence, torsion, and out-of-plane torsion angles, and nonbonded distances. D_e, α, and b_0 are empirical parameters for bond stretching (a Morse function), k_θ and θ_0 are empirical parameters for valence-angle bending, and k_χ is an empirical parameter for the out-of-plane deformational

(48) Comba, P.; Jakob, H.; Nuber, B.; Keppler, B. K. *Inorg. Chem*. **1994**, *33*, 3396−3400.
(49) Daul, C.; Niketić, S.; Rauzy, C.; Schläpfer, C. W. *Chem.−Eur. J.* **2004**, *10*, 721−727.
(50) Diaz-Acosta, I.; Baker, J.; Cordes, W.; Pulay, P. *J. Phys. Chem. A* **2001**, *105*, 238−244.
(51) Diaz-Acosta, I.; Baker, J.; Hinton, J. F.; Pulay, P. *Spectrochim. Acta, A* **2003**, *59*, 363−377.
(52) Becke, A. D. *J. Chem. Phys*. **1993**, *98*, 5648−5652.
(53) Lee, C.; Yang, W.; Parr, R. G. *Phys. Rev. B* **1988**, *37*, 785−789.
(54) Vosko, S. H.; Wilk, L.; Nusair, M. *Can. J. Phys*. **1980**, *58*, 1200−1211.
(55) Stephens, P. J.; Devlin, F. J.; Chabalowski, C. F.; Frisch, M. J. *J. Phys. Chem*. **1994**, *98*, 11623−11627.
(56) Mrak, Ž. M. Sc. Thesis, University of Zagreb, 1999.
(57) *Jaguar 5.0*; Schroedinger, L.L.C.: Portland, OR, 1991−2003.
(58) Hay, P. J.; Wadt, W. R. *J. Chem. Phys*. **1985**, *82*, 299−310.
(59) Ditchfield, R.; Hehre, W. J.; Pople, J. A. *J. Chem. Phys*. **1971**, *54*, 724.
(60) Hehre, W. J.; Pople, J. A. *J. Chem. Phys*. **1972**, *56*, 233.
(61) Binkley, J. S.; Pople, J. A. *J. Chem. Phys*. **1977**, *66*, 879.
(62) Hariharan, P. C.; Pople, J. A. *Theor. Chim. Acta*. **1973**, *28*, 213.
(63) Hehre, W. J.; Ditchfield, R.; Pople, J. A. *J. Chem. Phys*. **1972**, *56*, 2257.
(64) Francl, M. M.; Pietro, W. J.; Hehre, W. J.; Binkley, J. S.; Gordon, M. S.; DeFrees, D. J.; Pople, J. A. *J. Chem. Phys*. **1982**, *77*, 3654.
(65) Rassolov, V. A.; Pople, J. A.; Ratner, M. A.; Windus, T. L. *J. Chem. Phys*. **1998**, *109*, 1223.
(66) Chirlian, L. E.; Francl, M. M. *J. Comput. Chem*. **1987**, *8*, 894.
(67) Woods, R. J.; Khalil, M.; Pell, W.; Moffat, S. H.; Smith, V. H., Jr. *J. Comput. Chem*. **1990**, *11*, 297.
(68) Brenemann, C. M.; Wiberg, K. B. *J. Comput. Chem*. **1990**, *11*, 361.
(69) Reed, A. E.; Weinstock, E.; Weinhold, F. *J. Chem. Phys*. **1985**, *83*, 735−746.
(70) Glendening, E. D.; Badenhoop, J. K.; Reed, A. E.; Carpenter, J. E.; Bohmann, J. A.; Morales, C. M.; Weinhold, F. *NBO 5.0*; Theoretical Chemistry Institute, University of Wisconsin: Madison, WI, 2001.

potential. Torsional interactions are specified with V_φ and n (height and multiplicity of the torsional barrier, respectively). One torsion per bond was calculated. A and B are one-atom empirical parameters for the van der Waals interactions (a Lennard-Jones 12−6 function). q is a charge parameter. Intramolecular interactions separated by three and more bonds were considered nonbonded and calculated with the Lennard-Jones and electrostatic potentials. The interactions inside the metal(III) coordination sphere were modeled using the Morse potential between the metal and six oxygen donor atoms, and the repulsive electrostatic potential between the six oxygen atoms. It is a point-on-a-sphere model[71] without any explicit valence-angle bending potential for the angles around the metal ion.

All MM calculations were performed using the Lyngby version of the CFF program for conformational analysis,[72−74] which was slightly modified to cope with the electrostatic interactions between nonbonded atoms of the metal coordination polyhedron, and to treat more than 100 atoms in a molecule as well as in an asymmetric unit. In the Lyngby-CFF program, the input charge parameters can be used for an assignment of fractional atomic charges. The assignment is done by a special charge redistribution algorithm, which keeps the total charge of the molecules neutral and distributes the charge values in a manner supposed to mimic ab initio results.[74] The algorithm performs the following steps:[74] (1) the charges are assigned equal to the charge parameters, (2) the charges on the chain atoms are modified according to the charges on their side atoms [e.g., $q^{new}(C_{Me}) = q^{old}(C_{Me}) - {}^1/_3 q(H(C_{Me}))$, and $q^{new}(C_{pl}) = q^{old}(C_{pl}) - 0.8q(H(C_{pl}))$], (3) hydrogen atoms in strongly polar groups have reassigned charges depending on their chain atoms, (4) induction is taken into account [e.g., $q^{new}(O) = q^{old}(O) - 0.37q(C_{pl})$], (5) nonpolar groups (e.g., methylene) are neutralized, (6) the entire molecule is neutralized.

Two types of ab initio derived charges have been used in this work: the charges from the ESP fit and the charges yielded by NPA (see Quantum Chemical Calculations for details). It has been widely accepted that the ESP-based methods yield charges that depend strongly on the conformation and orientation of a molecule but are supposed to give the best description of the electrostatic properties of the molecule.[75] On the other side, the orbital-based methods, such as NPA, give charges that are independent of the orientation of a molecule and usually give the best chemical properties but are not well suited for use when electrostatic properties are of interest.[75] We used the charges from both schemes to construct two types of force fields to examine which force field type would yield a better fit with the experimental thermal properties.

The conformational potential energy was minimized for a molecule surrounded by other molecules in the crystal lattice (a condensed-phase approximation). The intermolecular atom−atom interactions were calculated using the same functional forms (Lennard-Jones 12−6 function and Coulombic potential, the only offered choice in the Lyngby-CFF program for modeling intermolecular interactions) and empirical parameters as for the intramolecular nonbonded interactions. The crystal simulations were carried out by using the Williams variant of the Ewald lattice summation method[76,77] with a spherical and abrupt cutoff limit of 14 Å, and convergence constants of 0.2 $Å^{-1}$, 0.2 $Å^{-1}$, and 0.0 for the Coulomb, dispersion, and repulsion lattice summation terms. The potential energy of a molecule in the crystal lattice, $V_{crystal}$, was calculated by adding to the intramolecular V_{total} potential energy the sum of intermolecular atom−atom interactions calculated between the atoms of the initial molecule and the atoms of all surrounding molecules within the cutoff limit. A detailed description of the crystal simulations is given elsewhere.[43,77] The empirical parameters of the potential energy functions were determined by combining trial and error guesses with the optimization algorithm, which is a variant of the general least-squares method (the Levenberg−Marquardt algorithm).[73,74]

3. Experimental Data for MM Modeling. The modeling included eight X-ray crystal structures of transition-metal(III) (Fe, Sc, Mn, Co, Cr, and V) complexes and one X-ray crystal structure of a non-transition-metal(III) (Al) complex with tris(acac)[18−25] (Table 1). The compounds are electrically neutral molecules. Their crystal structures consist of discrete molecules held together by van der Waals forces.

The crystal structures of the trivalent metal 2,4-pentandionato complexes appear to be grouped into several isomorphous series. They crystallize in either a monoclinic (the space groups $P2_1/c$ and $P2_1/n$) or an orthorhombic (the space groups $Pcab$ and $Pbca$) cell (Table 1). Both types of packing are obtained in the case of $V(acac)_3$, and two different monoclinic arrangements are present in the case of $Mn(acac)_3$ (Table 1).

In all selected $M(acac)_3$ complexes the chelate rings have very similar nearly planar geometry. The main difference between their molecular structures comes from the metal−oxygen distances, which range from 1.878 Å in $Co(acac)_3$[18] to 2.079 Å in $Sc(acac)_3$.[19] Here the special case is the two crystal forms of octahedral high-spin $3d^4$ Mn(III) structures susceptible to Jahn−Teller distortions.[24,25] The MnO_6 octahedron has a distinct tetragonal compression in $Mn(acac)_3$ (denoted also as β-$Mn(acac)_3$), with mean values for the axial and equatorial Mn−O bond lengths of 1.95 and 2.00 Å, respectively.[24] In γ-$Mn(acac)_3$, MnO_6 has a distinct tetragonal elongation, with average values for two axial Mn−O bond lengths of 2.111 Å and four equatorial Mn−O bond lengths of 1.945 Å.[25]

To check the force field's transferability, we searched the literature and the structural databases for metal complexes containing the same atom types as in the nine selected $M(acac)_3$ complexes. Tris(3-methyl-2,4-pentanedionato-*O*,*O*′)cobalt(III),[26] $Co(Me(acac))_3$, is the only such compound found. Its crystal form is triclinic (Table 1) with two unique complexes in an asymmetric unit. The geometry of the Me(acac) ligand was found similar to that observed for the acac ligand in $Co(acac)_3$, indicating minor steric influence of the central methyl group.

Results and Discussion

Thermochemical Properties. Table 2 presents the results of our calorimetric measurements for the tris(acac) complexes with Al(III), Fe(III), Cr(III), Mn(III), and Co(III) together with the enthalpies of fusion, $\Delta_{fus}H$, and the melting points, T^0, reported in other authors' papers.[27−32] The entropy of fusion, $\Delta_{fus}S$, has been calculated by dividing the enthalpy

(71) Hay, B. P. *Coord. Chem. Rev.* **1993**, *126*, 177−236.
(72) Niketić, S. R.; Rasmussen, Kj. *The Consistent Force Field: A Documentation*; Lectures Notes in Chemistry; Springer-Verlag: Berlin, Heidelberg, New York, 1977; Vol. 3.
(73) Rasmussen, Kj. *Potential Energy Functions in Conformational Analysis*; Lectures Notes in Chemistry; Springer-Verlag: Berlin, Heidelberg, New York, 1985; Vol. 37.
(74) Rasmussen, Kj.; Engelsen, S. B.; Fabricius, J.; Rasmussen, B. In *Recent Experimental and Computational Advances in Molecular Spectroscopy*; Fausto, R., Ed.; NATO ASI Series C: Mathematical and Physical Sciences; Kluwer Academic Publishers: Dordrecht, The Netherlands, 1993; Vol. 406, pp 381−419.
(75) Sigfridsson, E.; Ryde, U. *J. Comput. Chem.* **1998**, *19*, 377−395.
(76) Williams, D. E. *Top. Curr. Phys.* **1981**, *26*, 3−40.
(77) Pietilä, L.-O.; Rasmussen, Kj. *J. Comput. Chem.* **1984**, *5*, 252−260.

Table 1. Unit Cell Dimensions: Experimental (in Bold) and Calculated (Using Two Force Field Sets, FF-ESP and FF-NPA)

compd		*a*/Å	*b*/Å	*c*/Å	α/deg	*β*/deg	*γ*/deg	*V*/Å^3	space group	ref
Al(acac)$_3$	**exptl**	**14.069**	**7.568**	**16.377**	**90.00**	**99.00**	**90.00**	**1722.3**	***P*2$_1$/*c***	**18**
	FF-ESP	14.208	7.420	16.530	90.00	98.42	90.00	1723.9		
	FF-NPA	13.874	7.507	16.721	90.00	98.50	90.00	1722.3		
Sc(acac)$_3$	**exptl**	**15.380**	**13.730**	**16.720**	**90.00**	**90.00**	**90.00**	**3530.7**	***Pbca***	**19**
	FF-ESP	15.867	13.421	16.583	90.00	90.00	90.00	3531.5		
	FF-NPA	15.909	13.508	16.436	90.00	90.00	90.00	3531.9		
Fe(acac)$_3$	**exptl**	**15.471**	**13.577**	**16.565**	**90.00**	**90.00**	**90.00**	**3479.5**	***Pbca***	**20**
	FF-ESP	15.603	13.495	16.526	90.00	90.00	90.00	3479.9		
	FF-NPA	15.472	13.637	16.488	90.00	90.00	90.00	3478.8		
Cr(acac)$_3$	**exptl**	**14.031**	**7.551**	**16.376**	**90.00**	**99.06**	**90.00**	**1713.4**	***P*2$_1$/*c***	**21**
	FF-ESP	14.168	7.411	16.467	90.00	97.90	90.00	1712.6		
	FF-NPA	13.844	7.498	16.671	90.00	97.90	90.00	1714.0		
α-V(acac)$_3$	**exptl**	**15.447**	**16.623**	**13.502**	**90.00**	**90.00**	**90.00**	**3466.7**	***Pcab***	**22**
	FF-ESP	15.415	16.223	13.518	90.00	90.00	90.00	3380.4		
	FF-NPA	15.402	16.211	13.758	90.00	90.00	90.00	3434.9		
β-V(acac)$_3$	**exptl**	**16.340**	**13.060**	**8.108**	**90.00**	**90.00**	**90.00**	**1730.3**	***P*2$_1$/*n***	**23**
	FF-ESP	16.106	13.107	8.203	90.00	90.48	90.00	1731.5		
	FF-NPA	15.865	13.222	8.247	90.00	90.44	90.00	1729.9		
Mn(acac)$_3$	**exptl**	**14.013**	**7.600**	**16.373**	**90.00**	**99.33**	**90.00**	**1720.6**	***P*2$_1$/*c***	**24**
	FF-ESP	13.872	7.548	16.799	90.00	96.46	90.00	1747.6		
	FF-NPA	13.750	7.574	16.891	90.00	96.64	90.00	1747.3		
γ-Mn(acac)$_3$	**exptl**	**7.786**	**27.975**	**8.020**	**90.00**	**100.34**	**90.00**	**1718.5**	***P*2$_1$/*n***	**25**
	FF-ESP	7.653	27.310	8.216	90.00	102.31	90.00	1677.8		
	FF-NPA	7.694	27.264	8.322	90.00	102.78	90.00	1702.4		
Co(acac)$_3$	**exptl**	**13.951**	**7.470**	**16.222**	**90.00**	**98.29**	**90.00**	**1672.9**	***P*2$_1$/*c***	**18**
	FF-ESP	14.118	7.323	16.342	90.00	98.27	90.00	1672.1		
	FF-NPA	13.766	7.440	16.501	90.00	98.23	90.00	1672.5		
Co(Me(acac))$_3$	**exptl**	**8.040**	**15.151**	**16.458**	**108.08**	**90.97**	**96.48**	**1890.9**	***P*$\bar{1}$**	**26**
	FF-ESP	8.073	15.146	16.263	109.49	90.89	94.18	1867.9		
	FF-NPA	8.075	15.178	16.362	108.21	91.43	95.28	1893.9		

Table 2. Individual Measurements (in Italics) and Means and Standard Deviations of Enthalpies of Fusion, $\Delta_{fus}H$, Together with Melting Temperatures, T^0, Measured Using the DSC-1B Calorimeter (This Work) and from the Literature, and Calculated Entropies of Fusion, $\Delta_{fus}S = \Delta_{fus}H/T^0$ [a]

compd		this work	ref 27	ref 28	ref 29	ref 30	ref 31	ref 32
Al(acac)$_3$	$\Delta_{fus}H$	*36.15, 34.67, 35.26, 35.52, 34.39*						
		35.2 ± 0.6		32.7 ± 0.3	28.7 ± 1.3		33.7 ± 0.3	
	T^0	463.7		458			466.7	
	$\Delta_{fus}S$	75.9		71.4			72.2	
Fe(acac)$_3$	$\Delta_{fus}H$	*30.09, 30.05*						
		30.07 ± 0.02		34.1 ± 0.9				
		24.46, 26.61, 24.75[b]						
		25.3 ± 1.0[b]	25.9 ± 0.5			22.6 ± 0.5		
	T^0	458.8, 459.8[b]	454	455		462		454.3
	$\Delta_{fus}S$	65.5, 55.0[b]	57.0	74.9		48.9		
Cr(acac)$_3$	$\Delta_{fus}H$	*36.05, 36.26, 37.09, 35.84, 34.06*						
		35.9 ± 1.0	28.4 ± 0.5	35.2 ± 0.2		28.7 ± 1.3	34.0 ± 0.3	
	T^0	486.0	489	490		487	488.9	488
	$\Delta_{fus}S$	73.9	58.1	71.8		58.9	69.5	
Co(acac)$_3$[c]	ΔH	*90.85, 89.60, 101.28*[b]						
		93.9 ± 5.2[b]						
		52.54						
	T^0	478.1, 475.1[b]	503	475				513
	ΔS	109.9, 197.6[b]						
Mn(acac)$_3$	$\Delta_{fus}H$	*27.67*						
	T^0	421.9	455.5	447				445
	$\Delta_{fus}S$	65.6						
Sc(acac)$_3$	$\Delta_{fus}H$		28.8 ± 0.5					
	T^0		460	445				460.5
	$\Delta_{fus}S$		62.6					
V(acac)$_3$	$\Delta_{fus}H$		23.8 ± 0.5	30.0 ± 1.0				
	T^0		460	460				460.5
	$\Delta_{fus}S$		51.7	65.2				

[a] $\Delta_{fus}H$ is expressed in kJ mol^{-1}, T^0 in K, and $\Delta_{fus}S$ in J mol^{-1} K^{-1}. [b] Values measured on the TA Instruments DSC 2910 module with a standard sample pan. [c] The measured enthalpy contains the contributions of the enthalpy of fusion and enthalpy of decomposition.

of fusion by the corresponding melting temperature, i.e., $\Delta_{fus}S = \Delta_{fus}H/T^0$, and its values are also collected in Table 2.

The DSC results (Table 2) can be collected in two groups, with larger and smaller values of $\Delta_{fus}H$. The reason for this discrepancy can be understood by comparing the means of $\Delta_{fus}H$ we measured for Fe(acac)$_3$ on two different calorimeters, with and without high-pressure sample pans used. The larger $\Delta_{fus}H$ is similar to that obtained by Beech and

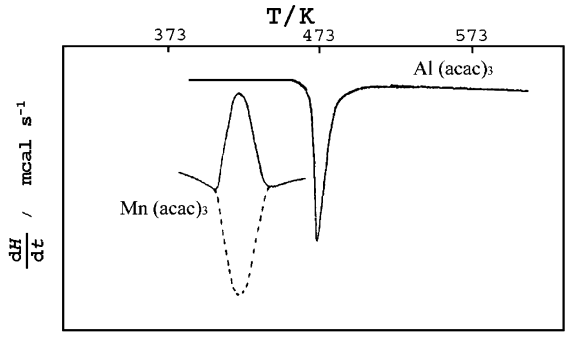

Figure 2. DSC measurements for $Al(acac)_3$ (a typical thermogram) and for $Mn(acac)_3$ (full line, the recorded thermogram; broken line, assumed thermogram representing fusion).

Lintonbon,[28] who used the same calorimeter type (DSC-1B) as we did. Similarly to our measurement system containing the closed high-pressure pan, Beech and Lintonbon filled empty space in the sample pan with aluminum, thus creating an internal heat sink and yielding more accurate measurements of thermal properties.[28] We obtained a smaller $\Delta_{fus}H = 25.3 \pm 1.0$ kJ mol^{-1} by recording the DSC thermogram of $Fe(acac)_3$ in a standard aluminum pan on the TA Instruments DSC 2910 module, thus without any means that could reduce the leaking of the volatile substance from the measuring system. The melting point for $Fe(acac)_3$ is very similar for both measuring conditions (Table 2).

For $Al(acac)_3$ (Figure 2), good reproducibility of the measurements with a standard deviation of 0.6 kJ mol^{-1} and good agreement with other reported data (Table 2) evidence the reliability of the result of $\Delta_{fus}H$ determination. $Al(acac)_3$ is fused without sublimation under atmospheric pressure. The melting point is in good agreement with previously reported values (Table 2).

Among all studied complexes, $Cr(acac)_3$ has the highest melting point (Table 2) and the lowest loss of mass (2.9%), so we may conclude that it is the thermally most stable complex. The enthalpy of fusion is in good agreement with the literature data as well as the melting point (Table 2).

Several unsuccessful attempts to measure $\Delta_{fus}H$ for $Mn(acac)_3$ and $Co(acac)_3$ have been reported.[27,28] Melia and Merrifield attributed the failure to determine the enthalpy of fusion for these two complexes to their decomposition.[27] Beech and Lintonbon interpreted the DSC curves of $Mn(acac)_3$ by the existence of two separate peaks, one belonging to the endothermic process and the second to the exothermic process:[28] the first endothermic peak in the DSC curve of the Mn(III) complex was described as sharp and characteristic of fusion; after the second exothermic peak a brown solid was formed which was analyzed for $Mn(acac)_2$. Beech and Lintonbon proposed the following processes to occur:[28] (1) the transformation of the solid state to the liquid phase of $Mn(acac)_3$ followed by (2) the transformation of liquid $Mn(acac)_3$ to crystalline $Mn(acac)_2$ with the transient existence of the gaseous 2,4-pentanedionyl radical, requiring a weight loss of 28.1%.

Unexpectedly, we succeeded in capturing a symmetrical DCS curve for $Mn(acac)_3$ (Figure 2) but unfortunately during only one calorimetric measurement. All our other attempted measurements on the instruments with either the high-pressure or the standard sample pan led to the two-step process as described by Beech and Lintonbon[28] with the melting point at 445.3 K.

The obtained DSC thermogram (Figure 2) describes the reaction that started as an endothermic one, turned toward the exothermic direction, and ended as an endothermic process. The fusion started at 421.9 K, which is a much lower temperature than usually recorded (Table 2). We suppose that the fusion's start at lower temperature was due to the pressure increase in the high-pressure closed sample pan, and that this action slowed process 2 proposed by Beech and Lintonbon. The weight loss of 17% vs 28.1% by Beech and Lintonbon[28] supports our supposition. However, we cannot offer an exact explanation for the process that turned the endothermic event into an exothermic one. We may suppose that in our DSC measurement a kind of crystal rearrangement might have happened that contributed to the exothermic process. As mentioned earlier, the $Mn(acac)_3$ complex was found in two monoclinic (β[24] and γ[25]) crystal modifications (Table 1). The molecule exhibits axial compression in β-$Mn(acac)_3$, whereas axial elongation is found in γ-$Mn(acac)_3$. The high-frequency and -field electron paramagnetic resonance spectroscopy measurements of the solid-state and frozen-solution structures of $Mn(acac)_3$ showed that the axial elongation could be considered the "natural" form of Jahn−Teller distortion for the octahedral high-spin electronic configuration of $3d^4$ ions.[78] The ab initio derived geometry of $Mn(acac)_3$ confirmed that the calculated Jahn−Teller distortion agreed well with the observed one in the γ-modification.[51] However, the magnetic measurements on $Mn(acac)_3$ by Gregson et al. revealed that the form they synthesized and studied was β-$Mn(acac)_3$.[79] The mechanism that triggers the molecular packing with either β or γ crystal modification is yet undetermined.

As the DSC thermogram for $Mn(acac)_3$ has a symmetrical shape (Figure 2), we could assume that the fusion did not stop but was screened by the exothermic process during the recorded thermochemical reaction. By reversing the exothermic peak, we obtained the assumed endothermic curve connecting the starting and ending points of the fusion (the broken line in Figure 2). The area under that symmetrical DSC curve (Figure 2) yielded the enthalpy value of 27.67 kJ mol^{-1}. To examine whether this value could be ascribed to the enthalpy of fusion, we performed solubility measurements of $Mn(acac)_3$.

The solubility of $Mn(acac)_3$ in acetylacetone was determined at temperatures, T, of 40, 50, and 60 °C. The corresponding measured solubilities are as follows: 28.33, 36.70, and 47.83 g of $Mn(acac)_3$/100 g of acetylacetone. Figure 3 compares experimental and theoretical dependencies between $\ln X_b$ and $(T^0 - T)/T$, where X_b is the mole fraction of solute in the saturation solution and T^0 is the melting

(78) Krzystek, J.; Yeagle, G. J.; Park, J.-H.; Britt, R. D.; Meisel, M. W.; Brunel, L.-C.; Telser, J. *Inorg. Chem.* **2003**, *42*, 4610−4618.
(79) Gregson, A. K.; Doddrell, D. M.; Healy, P. C. *Inorg. Chem.* **1978**, *17*, 1216−1219.

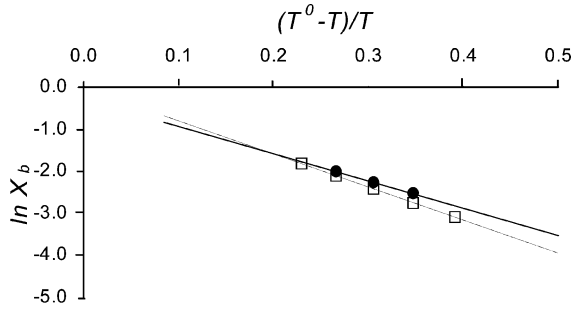

Figure 3. Solubility of Mn(acac)$_3$ in acetylacetone as a function of the $(T^0 - T)/T$ temperature ratio, $T^0 = 421.9$ K: (●) experimental data; (□) ln X_b predicted using the Clausius−Clapeyron equation with $\Delta_{fus}H = 27.67$ kJ mol^{-1}.

temperature. The theoretical dependence was calculated using the Clausius−Clapeyron equation:

$$\ln X_b = -\frac{\Delta_{fus}H}{RT^0}\frac{T^0 - T}{T}$$

where R is the gas constant and the experimental values of T^0 and $\Delta_{fus}H$ were used. Such comparison allowed probing the measured values of the melting point and enthalpy of fusion, and indeed, the good match between the experimental and theoretical lines (Figure 3) indirectly confirmed that 27.67 kJ mol^{-1} could be $\Delta_{fus}H$ of Mn(acac)$_3$.

For Co(acac)$_3$, the relatively large area under the DSC thermogram representing the enthalpy (Table 2) indicated that at least two simultaneous processes occurred, fusion and decomposition. The superposed processes in the overall thermogram prevent the determination of a meaningful and reliable $\Delta_{fus}H$ value for Co(acac)$_3$. Our DSC result coincides with that reported by Beech and Lintonbon.[28]

The variations in the $\Delta_{fus}S$ values (Table 2) obtained for the same compounds may be due to different measurement conditions under which the DSC thermograms have been recorded.

Force Field Parametrization. Having chosen the MM model, i.e., the potential energy functions, the next steps in the MM modeling of the selected M(acac)$_3$ complexes were deriving empirical parameters, calculation of equilibrium geometries, and adjustment of empirical parameters to get the best possible match between calculated and experimentally determined structural data.

In all nine X-ray crystal and molecular structures of M(acac)$_3$ selected for modeling (Table 1) the deviation from planarity of the six-membered chelate rings is small. Hence, the chelate ring planarity determined the torsion barrier multiplicity ($n = -2$) for the torsions around the O−C$_{pl}$, C$_{pl}$−C$_{pl}$, and M−O bonds (Figure 1) as well as holding the groups of four nonmetallic atoms in the plane by the out-of-plane deformation potential. The multiplicity for the torsion around the C$_{pl}$−C$_{Me}$ bond was set to 12 as in the copper(II) amino acid complexes[42−44] to be close to its usual experimental values. The equilibrium valence angles, θ_0, were selected according to their average values in the X-ray structures.

As mentioned in the Theoretical Methods, we used two charge types to construct the force fields. The means of the ESP and NPA charge values for chemically equivalent atoms in a molecule were calculated and were used as the guidelines for selecting the force fields' charge parameters. The charge parameters were varied until they yielded the fractional charge values assigned by Lyngby-CFF matched as close as possible with the means of the ESP and NPA charges. The force fields' charge parameters are given in Table S1 in the Supporting Information. The fractional charges assigned by the Lyngby-CFF program according to the charge parameters given in Table S1 are presented in Table S2 in the Supporting Information together with the ESP and NPA charges.

The initial values of all other parameters in the empirical parameter set were taken from the force field FFW[42,43] for copper(II) amino acidates. The charge parameters, q, the A and B Lennard-Jones parameters for hydrogen atoms, the Morse potential parameters for the C−H bonds, and all θ_0 and n values were kept unchanged, while other empirical parameters were optimized with respect to the experimental data (bond lengths, valence and torsion angles, and unit cell dimensions) of three transition-metal complexes with similar charge distributions, that is, Mn(acac)$_3$, Cr(acac)$_3$, and β-V(acac)$_3$. The parameter optimizations showed that the same A and B Lennard-Jones parameters should be used for C$_{pl}$ and C$_{Me}$ to get good reproduction of the unit cell dimensions. It also appeared that, when the NPA charges were used as a guideline for modeling electrostatic interactions, the Lennard-Jones parameters for C$_{Me}$ and the V_φ parameter for the torsion around the C$_{Me}$−C$_{pl}$ bond did not have to be modified to get a good match with the experimental structural data. These parameters could retain the values as in the FFW force field for copper(II) amino acidates (which also has the charge parameters selected to give the fractional charges close to the NPA values).[42,43] This fact as well as the very small change in k_θ for the H−C−H angle (from 310.000 kcal mol^{-1} rad^{-2} in FFW to 320.3024 kcal mol^{-1} rad^{-2} in this work, Table 3) points out the empirical parameters' transferability between two different classes of compounds for the valence-angle-bending, Morse and Lennard-Jones potentials describing the interactions within the methyl group.

Having approached a fairly good reproduction of the experimental structural data, we continued the fitting process with a finer selection of the parameters. We had two choices for the empirical parameters describing the M−O interaction, either to include the Morse potential parameters for this particular interaction into the fitting process for each metal complex separately or to choose identical values for all complexes. The first solution was ruled out for the following reasons: (1) it would encounter too many combinations of the parameter values that could yield good reproduction of the experimental structures, (2) we did not have enough experimental data to restrict the number of possible parameter combinations, and (3) different combinations of D_e, α, and b_0 would produce energy values unsuited for comparison. Namely, the main purpose of designing the modeling system was to examine a connection between experimental thermochemical data and the energy of M^{III}(acac)$_3$ complexes in the crystal state. Thus, we needed energy values whose

Table 3. Final Potential Energy Parameter Sets FF-ESP and FF-NPA for $M(acac)_3$ Complexes[a−c]

bond	force field	D_e	α	b_0
$C_{Me}-H$		101.6000	1.8000	1.0900
$C_{pl}-H$		101.6000	1.8000	1.0900
$C_{Me}-C_{pl}$		1334.1752	1.0000	1.5250
$C_{pl}-C_{pl}$		1586.3851	0.6702	1.3800
$C_{pl}-O$		28.2750	7.9744	1.2730
M−O	FF-ESP	246.0800	0.2570	2.0000
M−O	FF-NPA	246.0800	0.3570	1.1000

valence angle	k_θ	θ_0	valence angle	k_θ	θ_0
$H-C_{Me}-C_{pl}$	123.1944	1.9106	$C_{pl}-C_{pl}-H$	1263.3076	2.0769
$H-C_{Me}-H$	320.3024	1.9106	$O-C_{pl}-C_{Me}$	816.2954	2.0159
$C_{pl}-C_{pl}-O$	2091.1773	2.1729	$C_{pl}-C_{pl}-C_{Me}$	1530.0195	2.0944
$C_{pl}-C_{pl}-C_{pl}$	1711.7669	2.1293	$C_{pl}-O-M$	969.9777	2.2166

torsion angle	force field	V_φ	n
$M-O-C_{pl}-C_{Me}$		20.4259	−2.0000
$C_{pl}-C_{pl}-C_{pl}-C_{Me}$		19.8666	−2.0000
$H-C_{Me}-C_{pl}-C_{pl}$		0.7891	12.0000
$C_{pl}-O-M-O$	FF-ESP	7.4078	−2.0000
$C_{pl}-O-M-O$	FF-NPA	1.4078	−2.0000

out-of-plane torsion angle	k_χ	out-of-plane torsion angle	k_χ
$O(C_{pl}-C_{Me}-C_{pl})$	245.0000	$O(C_{pl}-C_{pl}-C_{Me})$	245.0000
$H(C_{pl})(C_{pl}-C_{pl}-C_{pl})$	245.0000	$C_{Me}(C_{pl}-C_{pl}-C_{pl})$	245.0000

nonbonding	force field	A	B
$H(C_{Me})$		80.0000	3.5810
$H(C_{pl})$		80.0000	3.5810
C_{Me}	FF-ESP	700.0000	15.0000
C_{Me}	FF-NPA	908.3580	13.8280
O	FF-ESP	800.0000	22.7500
O	FF-NPA	1700.0000	60.0000
C_{pl}	FF-ESP	700.0000	15.0000
C_{pl}	FF-NPA	908.3580	13.8280
Co(III)	FF-ESP	7000.0000	178.0000
Co(III)	FF-NPA	12300.0000	200.0000
Cr(III)	FF-ESP	16000.0000	165.0000
Cr(III)	FF-NPA	25000.0000	195.0000
Fe(III)	FF-ESP	25000.0000	165.0000
Fe(III)	FF-NPA	33000.0000	175.0000
Sc(III)	FF-ESP	42000.0000	170.0000
Sc(III)	FF-NPA	40000.0000	165.0000
Al(III)	FF-ESP	2600.0000	75.0000
Al(III)	FF-NPA	190.0000	17.5000
Mn(III)	FF-ESP	18000.0000	105.0000
Mn(III)	FF-NPA	30000.0000	100.0000
V(III)	FF-ESP	26000.0000	200.0000
V(III)	FF-NPA	31000.0000	170.0000

[a] The parameters without explicitly denoted force field have the same value in both force field types. [b] Uncommon symbols are denoted as in Figure 1: C_{pl}, planar carbon atom; C_{Me}, tetrahedral methyl group carbon; M, metal atom. [c] Units are as follows: D_e, kcal mol^{-1}; α, Å^{-1}; b_0, Å; k_θ, kcal mol^{-1} rad^{-2}; θ_0, rad; V_φ, kcal mol^{-1}; A, (kcal mol^{-1} Å^{12})$^{1/2}$; B, (kcal mol^{-1} Å^6)$^{1/2}$; k_χ, kcal mol^{-1} rad^{-2}.

comparison would be sound. For that reason we have selected a set of D_e, α, and b_0 values that could span the range of different M−O bond distances. Then, the A and B Lennard-Jones parameters for each M(III) were varied until a good fit was obtained between theoretical and experimental M−O bond lengths as well as unit cell dimensions. To sum up, different charge parameters for each $M(acac)_3$ complex and different A and B Lennard-Jones parameters for each M(III) were selected, while all other parameters were the same within the potential energy parameter set for all the complexes. Two potential energy parameter sets named FF-ESP and FF-NPA (where ESP and NPA denote the method for deriving charge values that were used in a corresponding force field) are given in Table 3.

FF-ESP vs FF-NPA. The use of different charges in the two force field sets yielded different values of the Lennard-Jones parameters for all atom types (other than hydrogen) in the first place. Additionally, to reproduce the M−O bond length range from 1.8 to 2.1 Å, different Morse parameters for the M−O bond had to be selected. Besides, a different empirical parameter for the torsion barrier, V_φ, had to be taken for the torsion around the M−O bond. Then good reproduction of the molecular and crystal structures was achieved using the same values for all other empirical parameters in both types of force fields (Table 3).

Reproduction of the Experimental Molecular and Crystal Structures of $M(acac)_3$. The unit cell dimensions calculated with the two force field sets are listed in Table 1. The comparison of the means of the experimental and theoretical M−O bond lengths and the valence angles around the metal atom are given in Tables 4 and 5. The root-mean-square (rms) deviations between experimental and calculated crystalline internal coordinates of the nine $M(acac)_3$ complexes and $Co(Me(acac))_3$ are presented in Table 6.

Both force fields FF-ESP and FF-NPA give very similar reproduction of the experimental crystal data (Table 1). The unit cell dimensions for the polymorphic $V(acac)_3$ and $Mn(acac)_3$ complexes are less well reproduced than for the other complexes (Table 1) because of the parametrization procedure. Namely, we tried to get the best possible reproduction of the α-$V(acac)_3$ and β-$V(acac)_3$ structures as well as of the $Mn(acac)_3$ and γ-$Mn(acac)_3$ structures with the same Lennard-Jones parameters used for V(III) and Mn(III) (Table 3), respectively. Despite that, the unit cell dimensions are very well reproduced by the two force fields as the relative errors range from −2.9% to +3.8% for the unit cell dimensions, and from −2.5% to +1.6% for the unit cell volumes.

Also good reproduction of the molecular geometries can be seen from relatively small rms deviations of the calculated internal coordinates from the experimental ones (Table 6). The overall rms deviations calculated over the internal coordinates of all nine $M(acac)_3$ complexes (Table 6) are quite comparable with the rms deviations obtained for anhydrous copper(II) amino acid complexes (i.e., rms(Δb) = 0.018 Å, rms($\Delta\theta$) = 2.1°, and rms($\Delta\varphi$) = 4.7°) for which a similar approach and the same functional forms were used in modeling crystal structures.[42]

The MM model simulates well the distorted octahedral metal(III) geometry as may be examined by comparing experimental and theoretical means of the MO_6 internal coordinates (Tables 4 and 5). Both force field sets reproduce the means of the experimental M−O bonds and most of the O−M−O angles within their standard deviation values (Tables 4 and 5). Besides, the force fields correctly reproduce the observed relation that the lengthening of the M−O bonds is in concert with the decrease of the intraring *cis* O−M−O angles,[18] although not to the full extent (Table 4).

Table 4. Means and Standard Deviations of Six M−O Bond Lengths and Three *cis* In-Ring O−M−O Valence Angles for Nine M(acac)$_3$ Complexes and Co(Me(acac))$_3$

	⟨M−O⟩/Å			⟨in-ring O−M−O⟩/deg		
compd	exptl	FF-ESP	FF-NPA	exptl	FF-ESP	FF-NPA
Sc(acac)$_3$	2.070(0.009)	2.068(0.005)	2.069(0.007)	82.0(0.3)	84.8(0.2)	85.4(0.4)
Fe(acac)$_3$	1.992(0.006)	1.991(0.004)	1.991(0.002)	87.0(0.2)	87.8(0.1)	88.0(0.1)
β-V(acac)$_3$	1.987(0.011)	1.987(0.001)	1.979(0.003)	87.4(0.3)	88.0(0.1)	88.4(0.0)
α-V(acac)$_3$	1.980(0.009)	1.983(0.002)	1.984(0.001)	87.8(0.4)	87.8(0.0)	88.2(0.1)
γ-Mn(acac)$_3$	1.993(0.083)	1.968(0.004)	1.980(0.005)	89.2(1.2)	88.7(0.1)	88.6(0.1)
Mn(acac)$_3$	1.981(0.030)	1.975(0.005)	1.983(0.006)	89.6(0.4)	88.6(0.2)	88.3(0.2)
Cr(acac)$_3$	1.956(0.007)	1.948(0.007)	1.959(0.007)	91.1(0.4)	89.6(0.2)	89.1(0.1)
Al(acac)$_3$	1.892(0.010)	1.886(0.006)	1.903(0.011)	91.8(0.1)	92.4(0.2)	92.3(0.5)
Co(acac)$_3$	1.898(0.019)	1.895(0.007)	1.903(0.009)	97.3(0.2)	91.6(0.3)	91.4(0.3)
Co(Me(acac))$_3$	1.875(0.006)	1.850(0.010)	1.881(0.010)	94.9(0.2)	93.7(0.3)	92.8(0.3)

Table 5. Means and Standard Deviations of Three *trans* O−M−O and Nine *cis* (Other Than In-Ring) O−M−O Valence Angles for Nine M(acac)$_3$ Complexes and Co(Meacac)$_3$

	⟨*cis* O−M−O⟩/deg			⟨*trans* O−M−O⟩/deg		
compd	exptl	FF-ESP	FF-NPA	exptl	FF-ESP	FF-NPA
Sc(acac)$_3$	93.0(3.2)	91.8(3.3)	91.6(3.5)	169.4(1.0)	174.8(2.0)	173.0(2.7)
Fe(acac)$_3$	91.1(2.6)	90.7(2.9)	90.7(3.4)	174.5(0.9)	175.6(0.5)	174.1(1.1)
β-V(acac)$_3$	90.9(1.7)	90.6(1.7)	90.6(2.9)	176.0(1.5)	177.3(0.9)	175.6(1.5)
α-V(acac)$_3$	90.8(1.9)	90.7(3.1)	90.7(4.3)	176.1(1.3)	175.7(2.0)	173.6(2.0)
γ-Mn(acac)$_3$	90.3(1.8)	90.4(2.6)	90.5(2.1)	177.4(2.0)	176.8(0.2)	176.6(1.1)
Mn(acac)$_3$	90.1(1.0)	90.5(4.0)	90.6(2.5)	178.5(0.4)	176.4(2.1)	177.0(0.8)
Cr(acac)$_3$	89.6(0.6)	90.2(4.6)	90.3(2.2)	178.6(0.8)	175.8(1.8)	177.6(0.6)
Al(acac)$_3$	89.4(1.2)	89.3(3.9)	89.2(1.4)	179.0(0.6)	174.3(2.9)	176.6(1.0)
Co(acac)$_3$	87.7(0.8)	89.6(4.8)	89.5(2.1)	173.6(0.4)	173.8(3.3)	176.3(0.8)
Co(Me(acac))$_3$	88.4(0.7)	88.8(1.7)	89.1(1.4)	175.6(0.6)	175.8(1.4)	177.5(0.8)

Table 6. Rms Deviations Calculated between Crystal Experimental and Theoretical (Derived Using the Two Force Field Sets FF-ESP and FF-NPA) Internal Coordinates for Each Complex Separately and over Nine M(acac)$_3$ Complexes[a]

	rms(Δb)/Å		rms($\Delta\theta$)/deg		rms($\Delta\varphi$)/deg		rms($\Delta\chi$)/deg	
compd	FF-ESP	FF-NPA	FF-ESP	FF-NPA	FF-ESP	FF-NPA	FF-ESP	FF-NPA
Al(acac)$_3$	0.028	0.028	2.8	1.6	2.8	2.3	2.1	2.1
Sc(acac)$_3$	0.014	0.015	3.5	2.8	5.4	5.1	2.6	1.6
Fe(acac)$_3$	0.017	0.019	2.2	1.6	4.1	3.7	2.2	1.8
Cr(acac)$_3$	0.017	0.012	2.4	1.5	2.9	2.8	1.8	1.6
α-V(acac)$_3$	0.011	0.012	1.9	2.0	3.2	3.3	1.2	0.8
β-V(acac)$_3$	0.027	0.024	1.8	1.5	4.7	3.9	2.2	1.8
Mn(acac)$_3$	0.027	0.027	2.1	1.6	4.9	4.8	4.2	3.9
γ-Mn(acac)$_3$	0.045	0.043	1.9	1.6	8.5	8.5	1.5	1.3
γ-Mn(acac)$_3$[b]	0.019	0.023	1.9	1.6	5.7	5.4	1.5	1.3
Co(acac)$_3$	0.024	0.023	3.9	3.4	2.7	2.4	2.5	2.5
overall	0.025	0.024	2.6	2.1	4.7	4.5	2.4	2.1
overall[b]	0.021	0.021	2.6	2.1	4.1	3.9	2.4	2.1
Co(Me(acac))$_3$	0.018	0.015	1.5	1.6	4.1	3.5	1.8	1.4

[a] Internal coordinates: bond lengths, b, valence angles, θ, torsion angles, φ, and out-of-plane torsion angles, χ. Hydrogen atoms are not used in the comparisons. [b] The rms deviations were calculated without accounting for two long Mn−O bond lengths as well as four distorted torsion angles (two O−Mn−O−C_{pl} angles and two Mn−O−C_{pl}−C_{Me} angles) in γ-Mn(acac)$_3$.

However, the MM model and the force fields cannot reproduce the extent of the Mn−O bond length variability for two high-spin Mn(III) complexes[24,25] susceptible to the Jahn−Teller distortions (Table 4). This is especially true for γ-Mn(acac)$_3$[25] in which the force fields cannot cover the 0.181 Å difference span between equatorial and axial Mn−O bond distances. This large Mn−O bond length variability seems to be connected with the most pronounced distortion from the chelate ring planarity (occurring in two chelate rings of γ-Mn(acac)$_3$)[25] among the studied M(acac)$_3$ complexes (Table 6). As the force fields keep the chelate rings close to the planar geometry in the theoretical structures, we may conclude that this caused the maximum error of 18.5° (for the C_{pl}−O−Mn−O torsion) in the reproduction of experimental torsion angles when considering all M(acac)$_3$. The maximum errors between experimental and FF-ESP values in bond lengths and valence angles for γ-Mn(acac)$_3$ are 0.146 Å (for Mn−O) and −4.5° (for O−Mn−O), respectively. The corresponding maximum deviations by FF−NPA are 0.135 Å (for the Mn−O bond length) and −3.6° (for the Mn−O−C_{pl} valence angle). The maximum deviations between experimental and theoretical internal coordinates (without taking into account those including hydrogen atoms) of the other eight M(acac)$_3$ complexes are as follows: 0.063 Å in the bond lengths (for C_{Me}−C_{pl} in Co(acac)$_3$) by both FF-ESP and FF−NPA, −8.8° (for O−Co−O) and −6.2° (for Co−O−C_{pl}) in the valence angles by FF-ESP and FF−NPA, respectively, and −11.2° (for O−V−O−C_{pl} in β-V(acac)$_3$) and −10.8° (for O−Mn−O−C_{pl}) in the torsion angles by FF-ESP and FF−NPA, respectively. The maximum errors

are also quite comparable with the maximum errors (−0.073 Å for bond lengths, −8.3° for valence angles, and −11.7° for torsion angles) obtained in the reproduction of the experimental crystalline internal coordinates of anhydrous copper(II) amino acidates.[42]

Reproduction of the Experimental Molecular and Crystal Structures of Co(Me(acac))$_3$. The transferability of the empirical parameters derived for the Co(acac)$_3$ complex (Tables 3 and S1) was tested on Co(Me(acac))$_3$. Application of the two Co(acac)$_3$ force fields on Co(Me(acac))$_3$ revealed the problem of correct fractional charge assignment by the Lyngby-CFF program as it gave a positive point charge value instead of the negative value on the central C_{pl} (the C_{pl} furthest away from the cobalt atom). Besides, the charge value obtained by the ESP procedure for Co(III) in Co(Me(acac))$_3$ was 0.607 e vs 1.438 e in Co(acac)$_3$. This difference in the fractional charge is too large and not easily reproducible by the charge redistribution algorithm. Conversely, the corresponding NPA charge values for Co(III) in the two complexes are nearly the same, i.e., 1.189 and 1.185 e. Hence, the Lyngby-CFF charge assignment was more easily and reliably reproducible for the NPA than for the ESP charges. For that reason, the charge redistribution routine of the Lyngby-CFF program was slightly changed (i.e., a few command lines were added to the subroutine, for, if C_{pl} is in certain positions in the molecule, then $q^{new}(C_{pl}) = 0.125q^{old}(C_{pl})$) to yield correct reproduction of the negative NPA charge value for C_{pl} furthest away from Co(III) using the FF-NPA charge parameters for Co(acac)$_3$ given in Table S1. The assigned fractional charges as well as ESP and NPA charges of Co(Me(acac))$_3$ are given in Table S2.

Both force fields developed for Co(acac)$_3$ reproduce well the unit cell dimensions of Co(Me(acac))$_3$ with relative errors of less than 2.5% (Table 1) as well as the internal coordinates of Co(Me(acac))$_3$ (Table 6), although FF-NPA slightly better than FF-ESP. FF-ESP reproduces the O−Co−O valence angles slightly better than FF-NPA (Tables 4 and 5), but only FF-NPA yields the average Co−O bond length to coincide with the experimental value within the standard deviation (Table 4). Thus, we can conclude that the empirical parameters developed for Co(acac)$_3$ (Tables 3 and S1) are capable of fulfilling the transferability property for Co(III) complexes containing the same atom types as Co(acac)$_3$. However, we must note that the transferability may be expected only if the same potential energy functions are used, and within the method approximations described in the MM Model and Calculations subsection.

Correlation between the Enthalpies of Fusion and Potential Energies of the Studied M(acac)$_3$ Complexes. The examination of a connection between calculated energies $V_{crystal}$ (Table 7) and the enthalpies of fusion included our values of $\Delta_{fus}H$ given in Table 2 for Al(acac)$_3$, Fe(acac)$_3$, Cr(acac)$_3$, and Mn(acac)$_3$. The $\Delta_{fus}H$ value for Co(acac)$_3$ was not taken into account because of the unreliability of its determination (Table 2). As the results of our DSC measurements are the closest to the Beech and Lintonbon ones,[28] we also included their $\Delta_{fus}H$ values (ref 28 in Table 2) in the correlation calculations. Figure 4 presents the correlations calculated between the FF-NPA $V_{crystal}$ energies and measured $\Delta_{fus}H$.

Table 7. In-Crystal Potential Energies, $V_{crystal}$, of Nine M(acac)$_3$ Complexes Calculated in the Simulated Crystalline Surroundings Using the Two Force Field Sets FF-ESP and FF-NPA[a]

	$V_{crystal}$/kJ mol^{-1}			$V_{crystal}$/kJ mol^{-1}	
compd	FF-ESP	FF-NPA	compd	FF-ESP	FF-NPA
Al(acac)$_3$	2129.5	0.0	β-V(acac)$_3$	1815.3	536.5
Sc(acac)$_3$	0.0	612.6	Mn(acac)$_3$	1965.5	737.3
Fe(acac)$_3$	1916.4	371.1	γ-Mn(acac)$_3$	1540.2	975.4
Cr(acac)$_3$	1738.7	540.4	Co(acac)$_3$	2404.5	271.8
α-V(acac)$_3$	948.5	668.8			

[a] The energies are calculated relative to −96953.6 kJ mol^{-1} (FF-ESP) and −92092.8 kJ mol^{-1} (FF-NPA).

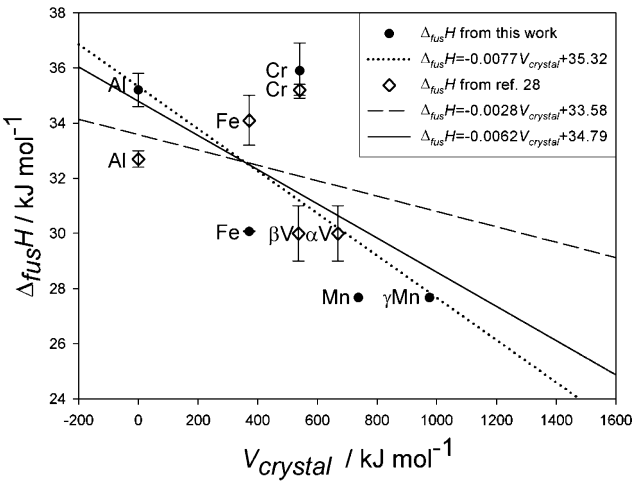

Figure 4. Correlations calculated between FF-NPA energies $V_{crystal}$ (data from Table 7) and enthalpies of fusion $\Delta_{fus}H$ (data from Table 2) from this work (dotted line, correlation coefficient $R = -0.71$), from ref 28 (broken line, $R = -0.31$), and from both this work and ref 28 (full line, $R = -0.60$).

The best correlation was obtained when $\Delta_{fus}H$ was taken only from this work (Figure 4). From the regression line calculated by taking into account $\Delta_{fus}H$ from this work as well as from both this work and ref 28 (Figure 4), we predicted $\Delta_{fus}H$ for Sc(acac)$_3$ to be 30.6 and 31.0 kJ mol^{-1}, respectively. The suggested values for Sc(acac)$_3$ are quite well in accord with our expectation that a somewhat greater value than reported in ref 27 (Table 2) should be obtained, thus proving that the derived correlation between FF-NPA $V_{crystal}$ and $\Delta_{fus}H$ is sound. Furthermore, from the dotted regression line (Figure 4) we predict the enthalpy of fusion for Co(acac)$_3$ (undetermined experimentally) to equal 33.2 kJ mol^{-1}.

We also calculated the correlations between the enthalpies of fusion and different potential energy contributions to FF-NPA $V_{crystal}$ (Table S3 in the Supporting Information). Compared to $V_{crystal}$, a more pronounced linear relationship with the $\Delta_{fus}H$ values from this work was obtained by the valence-angle-bending potential (correlation coefficient $R = -0.85$), bond-stretching potential ($R = -0.75$), and intermolecular energy ($R = -0.72$) contributions. The smallest correlation coefficient ($R = -0.10$) was yielded by the out-of-plane deformation potential, whose energy contribution to $V_{crystal}$ was also the smallest. The bond-stretching (Morse)

potential energy values contributed the most to the energy values of $V_{crystal}$ given in Table 7.

Conversely to the FF-NPA $V_{crystal}$ energies, the FF-ESP $V_{crystal}$ values (Table 7) correlated with $\Delta_{fus}H$ yielded points that were too scattered on the regression graph. The best correlation was obtained using $\Delta_{fus}H$ from ref 28 ($R = 0.50$, $\Delta_{fus}H = 0.0026V_{crystal} + 27.9$), while a rather small correlation coefficient ($R = 0.33$) was derived using $\Delta_{fus}H$ determined in this work, and an even smaller $R = 0.30$ was obtained when both this work and ref 28 $\Delta_{fus}H$ values were included in the correlation calculations.

Although our thermochemical results are the closest to the values reported in the Beech and Lintonbon paper[28] (Table 2), the correlation calculations showed quite marked correlation only when FF-NPA $V_{crystal}$ and $\Delta_{fus}H$ from this work were taken into account. The result points at the sensitivity of the correlation results to the differences in the $\Delta_{fus}H$ values derived for the same compounds, and indicates the necessity of controlled measurement conditions to get as reliable as possible $\Delta_{fus}H$ values of the M(acac)$_3$ complexes. On the other hand, the force field parametrizations influenced the in-crystal potential energy values used in the correlation calculations.

Conclusions

The measurements of thermodynamic properties using the DSC instrument with a high-pressure sample pan which prevented the leaking of volatile M^{III}(acac)$_3$ substances from the measuring system enabled reliable determination of $\Delta_{fus}H$ for Al(acac)$_3$, Fe(acac)$_3$, Cr(acac)$_3$ (in good agreement with earlier published values[28]), and Mn(acac)$_3$ for the first time.

The proposed MM model without an explicit valence-angle-bending potential for the O−M−O angles in M^{III}(acac)$_3$ complexes proves suitable for reproduction of the distorted octahedral geometry found in the experimental crystal structures. The transferability property of two force fields developed for Co(acac)$_3$ was successfully satisfied for Co(Me(acac))$_3$. Whereas both sets of force fields developed, FF-NPA and FF-ESP, reproduced well the experimental crystal and molecular structures of the nine M(acac)$_3$ complexes, only molecular in-crystal potential energies $V_{crystal}$ derived by FF-NPA yielded a marked correlation with the measured enthalpies of fusion. On the basis of these findings, we may conclude that the force fields containing the charges calculated using the NPA method are well suited for modeling this class of metal complexes in the crystalline surroundings, within the set of potential energy functions used and the method approximations employed as described in the MM Model and Calculation subsection.

The negative correlation ($R = -0.71$) between $\Delta_{fus}H$ and FF-NPA $V_{crystal}$ confirms our supposition that the relationship between these two physicochemical properties may be established. It points out that a more stable M(acac)$_3$ complex would have a larger enthalpy of fusion, which is in accord with chemical intuition.

Acknowledgment. Part of the study was financed by the Croatian Ministry of Science, Education and Sport (Grant No. 0022017).

Supporting Information Available: Listing of charge parameters of the FF-ESP and FF-NPA force fields (Table S1), partial atomic charges obtained by the ESP and NPA procedures and by the Lyngby-CFF program using the charge parameters from Table S1 (Table S2), and correlation coefficients resulting from correlation calculations between the enthalpies of fusion and potential energy contributions to FF-NPA $V_{crystal}$ (Table S3) (PDF). This material is available free of charge via the Internet at http://pubs.acs.org.

IC048900U